TECHNICAL ARTICLE

Crystal structure of morimotoite from Ice River, Canada

Sytle M. Antao[a)]
Department of Geoscience, University of Calgary, Calgary, Alberta T2N 1N4, Canada

(Received 10 February 2014; accepted 31 March 2014)

The crystal structure of a morimotoite garnet, ideally $Ca_3(Ti^{4+}Fe^{2+})Si_3O_{12}$, from the Ice River alkaline complex, British Columbia, Canada was refined by the Rietveld method, space group $Ia\bar{3}d$, and monochromatic synchrotron high-resolution powder X-ray diffraction (HRPXRD) data. Electron-microprobe analysis indicates a homogeneous sample with a formula $\{Ca_{2.91}Mg_{0.05}Mn^{2+}_{0.03}\}_{\Sigma 3}[Ti_{1.09}Fe^{3+}_{0.46}Fe^{2+}_{0.37}Mg_{0.08}]_{\Sigma 2}(Si_{2.36}Fe^{3+}_{0.51}Al_{0.14})_{\Sigma 3}O_{12}$. The HRPXRD data show a two-phase intergrowth. The reduced χ^2 and overall $R(F^2)$ Rietveld refinement values are 1.572 and 0.0544, respectively. The weight percentage, unit-cell parameter (Å), distances (Å), and site occupancy factors (sofs) for phase-1 are as follows: 76.5(1)%, a = 12.156 98(1) Å, average <Ca–O> = 2.4383, Ti–O = 2.011(1), Si–O = 1.693(1) Å, Ca(sof) = 0.943(2), Ti(sof) = 0.966(2), and Si(sof) = 1.095(3). The corresponding values for phase-2 are 23.5(1)%, a = 12.160 67(2) Å, average <Ca–O> = 2.452, Ti–O = 1.988(3), Si–O = 1.704(3) Å, Ca(sof) = 1.063(7), Ti(sof) = 1.187(7), and Si(sof) = 1.220(8). The two phases cause strain that arises from structural mismatch and gives rise to low optical anisotropy. Because the two phases are structurally quite similar, a refinement using a single-phase model with anisotropic displacement parameters shows no unusual displacement ellipsoid for the O atom that requires a "split O-atom position", as was done in previous studies. © *2014 International Centre for Diffraction Data.* [doi:10.1017/S0885715614000414]

Key words: garnet, morimotoite, optical anisotropy, two-phase intergrowth, Rietveld refinements, synchrotron high-resolution powder X-ray diffraction (HRPXRD), crystal structure

I. INTRODUCTION

Peterson *et al.* (1995) observed unusual and large anisotropic displacement parameters for the O atom on a single position for morimotoite garnet from Ice River. So, they modeled a split position for the O atom and used isotropic displacement parameters. The reason for these unusual displacement parameters was attributed to different size Si and Fe atoms on the tetrahedral site. Attempts were made to show that the SiO_4 and the O_4H_4 tetrahedra in hydrogarnets have different sizes by also using a "split O-atom position" model, which was also used to explain the unusual anisotropic displacement ellipsoid of the O atom that elongate along the "Si–O" bond instead of right angles to this bond direction (e.g. Figure 2 in Armbruster, 1995; Figure 2 in Ferro *et al.*, 2003). These unusual features of the O-atom displacement ellipsoid may be the result of multi-phase intergrowths and are investigated in this study with regard to morimotoite and have implications for hydrogarnets.

Recently, we proposed that a multi-phase intergrowth of two or three cubic phases with slightly different structural (and chemical) parameters gives rise to strain arising from structural mismatch, and that this strain is the cause of the anisotropy in cubic garnets (Antao, 2013a, 2013b, 2013c; Antao and Klincker, 2013a, 2013b; Antao and Round, 2014). This explanation is tested further in this study for morimotoite because Ti-rich andradites are known to be birefringent, but their structures were refined in the cubic space group (e.g. Armbruster *et al.*, 1998).

The crystal structure of many members of the garnet group have been refined (e.g. Novak and Gibbs, 1971; Lager *et al.*, 1989; Armbruster and Geiger, 1993). The general formula for garnet is $^{[8]}X_3{}^{[6]}Y_2{}^{[4]}Z_3{}^{[4]}O_{12}$, Z=8, space group $Ia\bar{3}d$, where the eight-coordinated dodecahedral X site contains Mg^{2+}, Ca^{2+}, Mn^{2+}, or Fe^{2+} cations, the six-coordinated octahedral Y site contains Al^{3+}, Cr^{3+}, Fe^{3+}, Ti^{4+}, or Zr^{4+} cations, and the four-coordinated tetrahedral Z site contains Si^{4+}, Fe^{3+}, or Al^{3+} cations, or (O_4H_4) (e.g. Armbruster *et al.*, 1998). The structure of garnet consists of alternating ZO_4 tetrahedra and YO_6 octahedra with X atoms filling cavities to form XO_8 dodecahedra. The eight O atoms in the XO_8 dodecahedron occur at the corners of a distorted cube.

This study examines the crystal structure of a morimotoite, $\{Ca_{2.91}Mg_{0.05}Mn^{2+}_{0.03}\}_{\Sigma 3}[Ti_{1.09}Fe^{3+}_{0.46}Fe^{2+}_{0.37}Mg_{0.08}]_{\Sigma 2}(Si_{2.36}Fe^{3+}_{0.51}Al_{0.14})_{\Sigma 3}O_{12}$, from Ice River using high-resolution powder X-ray diffraction (HRPXRD) data that show a two-phase intergrowth that causes strain, which gives rise to low optical anisotropy. Moreover, a refinement of a single-phase model with anisotropic displacement parameters shows no unusual features for the O atom that requires a "split O-atom position" model.

II. EXPERIMENTAL

A. Sample characterization and electron-microprobe analysis (EMPA)

The black morimotoite sample is from the Ice River alkaline intrusive complex, Yoho National Park, British Columbia, Canada. The same sample was studied by Locock *et al.* (1995) and Peterson *et al.* (1995). A thin section

a)Author to whom correspondence should be addressed. Electronic mail: antao@ucalgary.ca

of the sample shows weak optical anisotropy under cross-polarized light.

The morimotoite sample was analyzed with a JEOL JXA-8200 wavelength-dispersive (WD)–ED electron-microprobe analyzer. The JEOL operating program on a Solaris platform was used for ZAF (atomic number, absorption, fluorescence) correction and data reduction. The WD operating conditions were 15 kV, 20 nA, 5 μm beam diameter, and using various standards [almandine-pyrope (Mg$K\alpha$), grossular (Ca$K\alpha$), almandine (Fe$K\alpha$, Al$K\alpha$, Si$K\alpha$), rutile (Ti$K\alpha$), spessartine (Mn$K\alpha$), and chromite (Cr$K\alpha$)]. The sample appeared homogeneous based on optical observations and EMPA results of eight spots from different areas of a crystal with a diameter of about 2 mm. The EMPA data were analyzed using the spreadsheet developed by Locock (2008) and the average chemical composition is given (Table I).

TABLE I. EMPA results for morimotoite.

Oxide (wt.%)	This study	Locock *et al.* (1995)	Henmi *et al.* (1995)
SiO_2	27.47(12)	27.42	26.93(12)
TiO_2	16.83(15)	16.43	18.51(17)
ZrO_2	n.d.	0.93	1.48(12)
Al_2O_3	1.33(5)	1.36	0.97(5)
Cr_2O_3	0.04(1)	0.00	
V_2O_3	n.d.	0.20	
FeO_{tot}	18.66(9)	5.14	7.78(3)
Fe_2O_3(calc.)			11.42(37)
MnO	0.47(3)	0.44	0.23(3)
MgO	1.00(2)	1.06	0.87(4)
CaO	31.65(14)	31.24	31.35(16)
Na_2O	n.d.	0.23	
H_2O^+	n.d.	0.04	
$\sum$	97.43	99.54	99.54
Recalc. (wt.%)			
Final FeO	5.17(21)	5.14	7.78(3)
Final Fe_2O_3	14.99(26)	15.05	11.42(37)
$\sum$(calc.)	98.94	99.54	99.54
Cations for 12 O atoms			
Mn^{2+}	0.034(2)	0.032	0.017
Mg^{2+}	0.053(9)	0.068	0.091
Ca^{2+}	2.913(8)	2.862	2.893
Na^{1+}	0.000	0.038	0.000
$\sum$X	3.000	3.000	3.000
Ti^{4+}	1.087(9)	1.057	1.199
Zr^{4+}	0.000	0.039	0.062
Cr^{3+}	0.002(1)	0.000	0.000
V^{3+}	0.000	0.014	0.000
Fe^{2+}	0.371(15)	0.368	0.560
Fe^{3+}	0.463(15)	0.456	0.157
Mg^{2+}	0.075(8)	0.067	0.021
$\sum$Y	2.000	2.000	2.000
Si^{4+}	2.359(10)	2.345	2.319
Al^{3+}	0.135(5)	0.137	0.098
Fe^{3+}	0.506(11)	0.513	0.583
H_4	0.000	0.006	0.000
$\sum$Z	3.000	3.000	3.000
End-members mole %			
Kimzeyite	0.00	1.94	3.11
Schorlomite	25.28	25.63	29.13
Al-schorlomite	6.75	4.91	1.82
Morimotoite	**37.15**	**36.76**	**56.03**
NaTi garnet	0.00	1.91	0.00
Mg-morimotoite	7.54	4.03	2.00
Goldmanite	0.00	0.69	0.00
Uvarovite	0.12	0.00	0.00
Andradite	20.26	20.81	4.34
Calderite	1.14	1.06	0.56
Khoharite	1.76	0.92	2.98
Remainder	0.00	1.35	0.05
$\sum$	100.00	100.01	100.02
Quality index	Superior	Excellent	Superior

Numbers in bold indicate the dominant end-member morimotoite, ideally $Ca_3(Ti^{4+}Fe^{2+})Si_3O_{12}$, so all three samples are called morimotoite.

B. Synchrotron HRPXRD

The morimotoite sample was studied by HRPXRD that was performed at beamline 11-BM, Advanced Photon Source, Argonne National Laboratory. A small fragment (about 2 mm in diameter) of the sample was crushed to a fine powder using an agate mortar and pestle. The crushed sample was loaded into a Kapton capillary (0.8 mm internal diameter) and rotated during the experiment at a rate of 90 rotations per second. The data were collected at 23 °C to a maximum 2θ of about 50 with a step size of 0.001° and a step time of 0.1 s per step. The HRPXRD trace was collected with 12 silicon (111) crystal analyzers that reduce the angular range to be scanned and allow rapid acquisition of data. A silicon (NIST 640c) and alumina (NIST 676a) standard (ratio of ⅓ Si:⅔ Al_2O_3 by weight) was used to calibrate the instrument and refine the monochromatic wavelength used in the experiment (see Table II). Additional details of the experimental setup are given elsewhere (Antao *et al.*, 2008; Lee *et al.*, 2008; Wang *et al.*, 2008).

C. Rietveld structure refinements

The HRPXRD data were analyzed by the Rietveld (1969) method, as implemented in the *GSAS* program (Larson and Von Dreele, 2000), and using the *EXPGUI* interface (Toby, 2001). Scattering curves for neutral atoms were used. The starting atom coordinates, cell parameter, and space group, $Ia\bar{3}d$, were taken from Peterson *et al.* (1995). The background was modeled using a Chebyschev polynomial (eight terms). The reflection-peak profiles were fitted using type-3 profile in the *GSAS* program. A full-matrix least-squares refinement was carried out by varying the parameters in the following sequence: a scale factor, unit-cell parameter, atom coordinates, and isotropic displacement parameters. Examination of the HRPXRD trace for morimotoite shows the presence of two separate phases with slightly different unit-cell parameters (Figures 1 and 2). Both the HRPXRD trace and the Rietveld refinement statistics indicate that the two-phase model is preferred over the single-phase model (Table II). The two separate phases were refined together with the site occupancy factors (sofs) in terms of the dominant Ca, Ti, and Si atoms in the corresponding X, Y, and Z sites. Toward the end of the refinement, all the parameters were allowed to vary simultaneously, and the refinement proceeded to convergence. A single-phase model was also refined using anisotropic displacement parameters to check for unusual O-atom features that were reported by Peterson *et al.* (1995).

The cell parameters and the Rietveld refinement statistics for the single- and two-phase models are listed in Table II. Atom coordinates, isotropic displacement parameters, and sofs are given in Table III. Anisotropic displacement parameters for the single-phase model are given in Table IV. Bond distances are given in Table V.

TABLE II. HRPXRD data and Rietveld refinement statistics for morimotoite.

	This study		
	Single phase[a]	Phase-1	Phase-2
wt.%	100	76.5(1)	23.5(1)
a (Å)	12.157 90(1)	12.156 98(1)	12.160 67(2)
Δa (Å)[b]	–	–	−0.0037
Reduced χ^2	1.663	1.572	
$R(F^2)$[c]	0.0514	0.0544	
wRp	0.0733	0.0651	
N_{obs}	701	1388	
2θ range	2–50°		
λ (Å)	0.413 38(2)		
Data points	47 992		

[a]Based on anisotropic displacement parameters.
[b]The strain and birefringence are proportional to $\Delta a = (a_{\text{dominant phase}} - a_{\text{minor phase}})$ (Kitamura and Komatsu, 1978).
[c]$R(F^2)$ = overall R-structure factor based on observed and calculated structure amplitudes = $[\sum(F_o^2 - F_c^2)/\sum(F_o^2)]^{1/2}$.

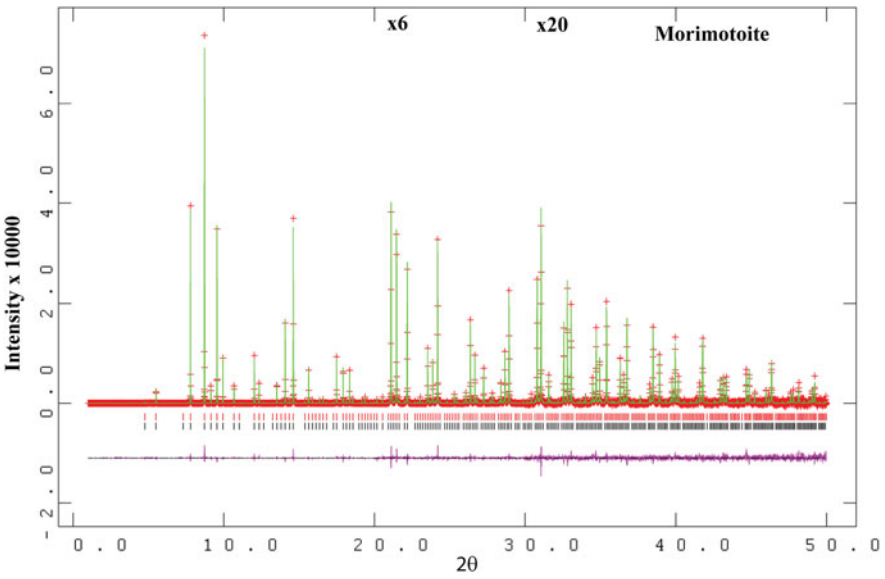

Figure 1. (Color online) HRPXRD trace for morimotoite (two-phase model) together with the calculated (continuous line) and observed (crosses) profiles. The difference curve ($I_{obs} - I_{calc}$) is shown at the bottom. The short vertical lines indicate allowed reflection positions. The intensities for the trace and difference curve that are above 20° and 30° 2θ are multiplied by factors of 6 and 20, respectively.

III. RESULTS AND DISCUSSION

The composition for the Ice River sample, $\{Ca_{2.91}Mg_{0.05}Mn^{2+}_{0.03}\}_{\Sigma 3}[Ti_{1.09}Fe^{3+}_{0.46}Fe^{2+}_{0.37}Mg_{0.08}]_{\Sigma 2}(Si_{2.36}Fe^{3+}_{0.51}Al_{0.14})_{\Sigma 3}O_{12}$, shows the distribution of the atoms in the three cation sites indicated by the general formula $^{[8]}X_3{}^{[6]}Y_2{}^{[4]}Z_3{}^{[4]}O_{12}$ (Table I). Using the data from Locock *et al.* (1995) and recalculating the cation content using the spreadsheet from Locock (2008), their composition, $\{Ca_{2.86}Mg_{0.07}Na_{0.04}Mn^{2+}_{0.03}\}_{\Sigma 3}[Ti_{1.06}Fe^{3+}_{0.46}Fe^{2+}_{0.37}Mg_{0.07}Zr_{0.04}V_{0.01}]_{\Sigma 2}(Si_{2.35}Fe^{3+}_{0.51}Al_{0.14})_{\Sigma 3}O_{12}$, is similar to that obtained in this study, as expected (Table I). Similarly, the composition, $\{Ca_{2.89}Mg_{0.09}Mn^{2+}_{0.02}\}_{\Sigma 3}[Ti_{1.20}Fe^{3+}_{0.16}Fe^{2+}_{0.56}Mg_{0.02}Zr_{0.06}]_{\Sigma 2}(Si_{2.32}Fe^{3+}_{0.58}Al_{0.10})_{\Sigma 3}O_{12}$, was obtained for the type material from Japan (Henmi *et al.*, 1995). The ideal end-member formula for morimotoite is $Ca_3(Ti^{4+}Fe^{2+})Si_3O_{12}$, which is the dominant component in the chemical analysis, so all three samples are called morimotoite (Table I). The Ice River sample was previously called schorlomite (Peterson *et al.*, 1995; Locock, 2008). However, the dominant component in Table I is morimotoite, which is the name used in this study and in Grew *et al.* (2013).

The reduced χ^2 and overall $R(F^2)$ Rietveld refinement values are 1.572 and 0.0544, respectively, for the two-phase model and they are similar to those for the single-phase model (Table II). The sofs obtained from the refinement are similar to those calculated from the EMPA results (Table III). The bond distances calculated from the atom radii are similar to those obtained from the Rietveld structure refinements (Table V).

The unit-cell parameter for the Ice River sample [a = 12.157 90(1) Å] is smaller than a = 12.162(3) (Å) for the type-material morimotoite from Japan (Henmi *et al.*, 1995), for which no structural data are available. However, the bond distances calculated from the atom radii are similar to the other samples (Table V). The reason for the larger cell for the type material seems to be the larger amount of Fe^{2+} in the Y site and the slightly longer cation–O distances (Table V).

The single-crystal results from Peterson *et al.* (1995) using one O-atom position for the same morimotoite sample matches the single-phase HRPXRD results from this study (Table V). However, Peterson *et al.* (1995) observed unusual displacement parameters for the O atom with its displacement ellipsoid elongated along the "Si–O" bond. So, they modeled a split position for the O atom. Attempts were also made to show that the SiO_4 and the O_4H_4 tetrahedra in hydrogarnets have different

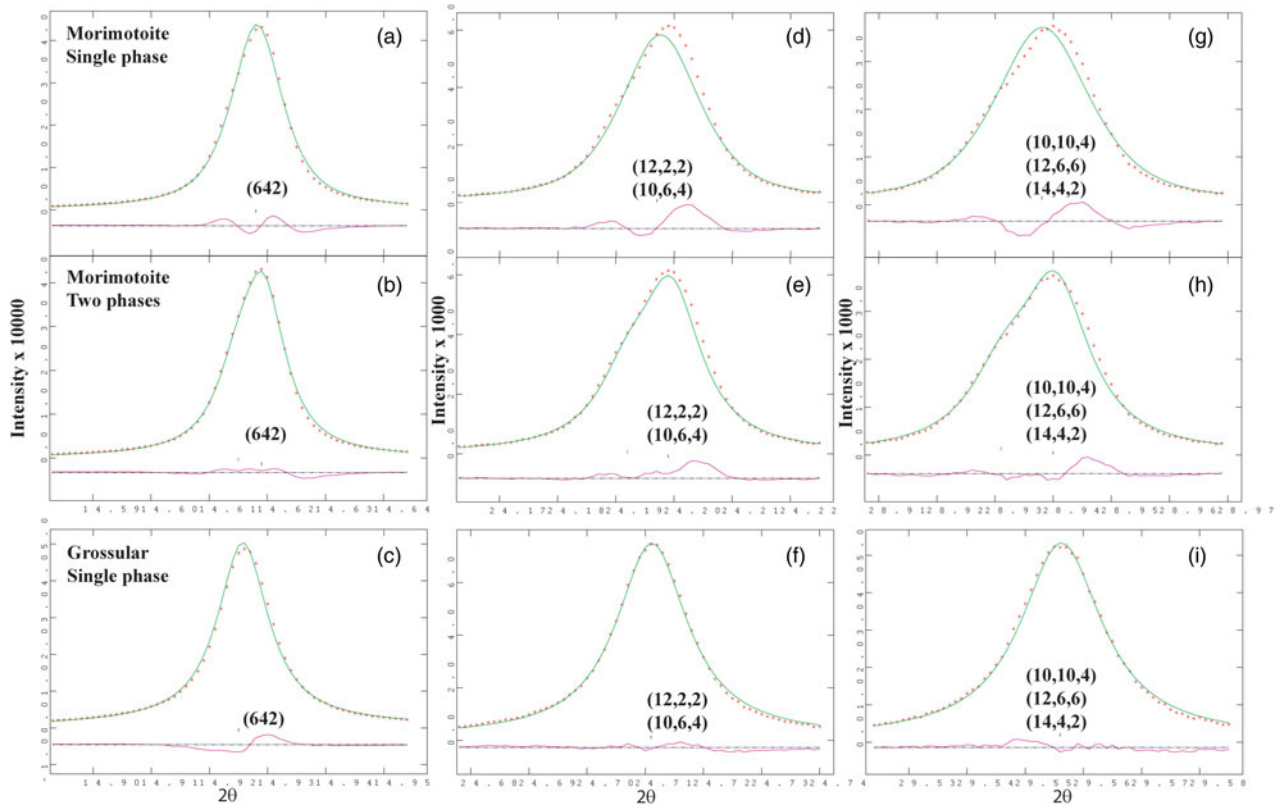

Figure 2. (Color online) A comparison of the same reflections in morimotoite and grossular. Parts (a), (d), and (g) are morimotoite data fitted using a single phase. Parts (b), (e), and (h) are morimotoite data fitted using two phases. Parts (c), (f), and (i) are grossular data fitted using a single phase for comparison (Antao, 2013a). The two phases for morimotoite fit the data best and matches the left shoulder on the high-angle peaks. The peaks in grossular are narrower than those in morimotoite.

sizes by using a "split O-atom position" model, which was used to explain the unusual displacement ellipsoid of the O atom that also elongates along the "Si–O" bond (e.g. Lager *et al.*, 1987; Armbruster and Lager, 1989; Ferro *et al.*, 2003).

A single-phase model for the Ice River sample was refined using anisotropic displacement parameters to test the "split O-atom position" hypothesis (Table IV). No unusual O-atom features were observed, as shown by the tetrahedral

TABLE III. Atom coordinates[a], isotropic displacement parameters (U, $Å^2$)[b], and sofs for morimotoite.

		This study			Peterson *et al.* (1995)
		Single phase[c]	Phase-1	Phase-2	
Ca(X)	U	0.009 53(3)	0.008 84(9)	0.008 84(9)	0.0061(9)
Ti(Y)	U	0.005 95(3)	0.005 53(5)	0.005 53(5)	0.0070(3)
Si(Z)	U	0.005 88(3)	0.0072(1)	0.0072(1)	0.012(1)
O	x	0.037 06(4)	0.036 77(8)	0.0379(2)	0.0368(4)
	y	0.048 51(4)	0.048 60(8)	0.0484(2)	0.0488(4)
	z	0.653 20(4)	0.653 80(8)	0.6515(2)	0.6528(4)
	U	0.013 31(3)	0.0155(2)	0.0155(2)	0.011(2)
Ca(X)	sof	0.985(1)	0.943(2)	1.063(7)	
Ti(Y)	sof	1.035(1)	0.966(2)	1.187(7)	
Si(Z)	sof	1.131(1)	1.095(3)	1.220(8)	
Ca(X)	EMPA sof	0.996	0.996	0.996	0.988
Ti(Y)	EMPA sof	1.059	1.059	1.059	1.076
Si(Z)	EMPA sof	1.141	1.141	1.141	1.141
X	Δ(sof)[d]	−0.01	−0.05	0.07	
Y	Δ(sof)	−0.02	−0.09	0.13	
Z	Δ(sof)	−0.01	−0.05	0.08	
X	Δe[e]	−0.22	−1.06	1.34	
Y	Δe	−0.53	−2.05	2.82	
Z	Δe	−0.14	−0.64	1.11	

[a]X at (0, ¼, ⅛), Y at (0, 0, 0), and Z at (⅜, 0, ¼). The O(sof) = 1 in all cases.
[b]U parameter for the same site in phases 1 and 2 were constrained to be equal.
[c]Data are from a refinement using isotropic displacement parameters.
[d]Δ(sof) = sof (HRPXRD refinement)−sof (EMPA).
[e]Δe = electrons (HRPXRD refinement)−electrons (EMPA).

TABLE IV. Anisotropic displacement parameters (Å^2) for single-phase morimotoite.

	U_{eq}	U_{11}	U_{22}	U_{33}	U_{12}	U_{13}	U_{23}
Ca(X)	0.0091	0.0108(1)	0.0108(1)	0.0058(2)	0.0042(2)	0	0
Ti(Y)	0.0058	0.005 77(4)	0.005 77(4)	0.005 77(4)	0.0005(1)	0.0005(1)	0.0005(1)
Si(Z)	0.0066	0.0065(3)	0.0067(1)	0.0067(1)	0	0	0
O	0.0142	0.0187(3)	0.0117(3)	0.0123(3)	−0.0025(3)	0.0041(2)	−0.0030(2)

TABLE V. Selected distances (Å) and angle (°) for morimotoite.

		This study			Peterson *et al.* (1995)	Henmi *et al.* (1995)
		Single phase[a]	Phase-1	Phase-2		
a (Å)		12.157 90(1)	12.156 98(1)	12.160 67(2)	12.157(3)	12.162(3)
Z–O	×4	1.6958(5)	1.693(1)	1.704(3)	1.703(5)	
Y–O	×6	2.0050(5)	2.011(1)	1.988(3)	2.000(5)	
X–O	×4	2.3696(5)	2.3631(9)	2.388(3)	2.370(5)	
X–O	×4	2.5143(5)	2.5134(9)	2.515(3)	2.510(5)	
<X–O>	[8]	2.442	2.438	2.452	2.440	
<D–O>[b]		2.146	2.145	2.149	2.146	
Y–O–Z		133.16(3)	132.88(5)	133.9(2)		
Radii ∑						
Z–O		1.68			1.68	1.69
Y–O		2.03			2.01	2.02
<X–O>		2.44			2.42	2.43
<D–O>		2.15			2.14	2.14

[a]Data are from a refinement using isotropic displacement parameters.
[b]<D–O> = {(Z–O) + (Y–O) + (X–O) + (X′–O)}/4. For the calculated bond distances, the following radii from Shannon (1976) were used (X site: Mn^{2+} = 0.96, Mg^{2+} = 0.89 Å; Y site: Ti^{4+} = 0.605, Cr^{3+} = 0.615, Fe^{2+} = 0.78, Fe^{3+} = 0.645, Mg^{2+} = 0.72 Å; Z site: Si^{4+} = 0.26, Al^{3+} = 0.39, Fe^{3+} = 0.49 Å). Ca^{2+} = 1.06 Å instead of 1.12 Å; this gives more realistic <X–O> distances.

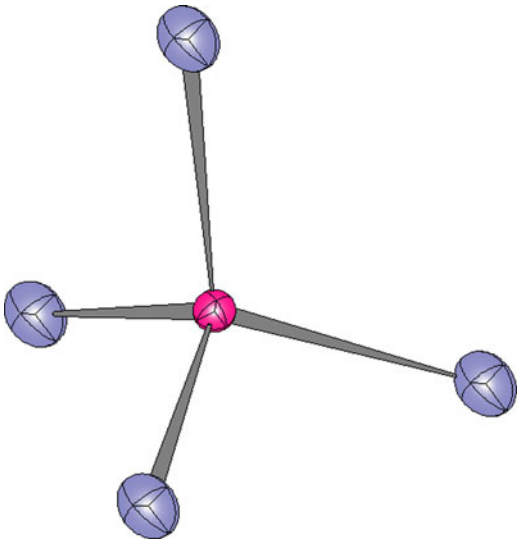

Figure 3. (Color online) Tetrahedral coordination of the Z site showing that the O atoms are not elongated along the "Si–O" bond direction, as was found by Peterson *et al.* (1995).

coordination of the Z site by O atoms (Figure 3). The displacement parameter for the Z site is about the same as that for the Y site and both are smaller than that for the X site (Table III). However, Peterson *et al.* (1995) obtained displacement parameters for the Z site that are larger than those of the X and Y sites, which is usual (Table III). It is possible that multiphase intergrowths may give rise to unusual ellipsoids for the O atom, if the unit-cell parameters for the phases are quite different from each other (e.g. Koritnig *et al.*, 1978; Antao, 2013c), which is not the case in this study.

The sample used in this study may contain a two-phase intergrowth instead of a single phase. The same reflections are compared for: (1) a single-phase [Figures 2(a), 2(d), and 2(g)]; (2) a two-phase [Figures 2(b), 2(e), and 2(h)]; and (3) a single-phase grossular [Figures 2(c), 2(f), and 2(i); data from Antao, 2013a]. No significant differences are observed for the low-angle peak near 14.9°. However, from the two high-angle peaks [near 24° and 29° 2θ in Figures 2(e) and 2(h)], it appears that the Ice River sample is a two-phase intergrowth. The trace for grossular contains only one peak for each reflection [Figures 2(c), 2(f), and 2(i)]. The two phases in morimotoite have slightly different unit-cell parameters: a = 12.156 98(1) for phase-1 and a = 12.160 67(2) for phase-2. Although splitting of the reflections is difficult to observe in this study, they are easily observed in other studies (e.g. Koritnig *et al.*, 1978; Antao, 2013c). The residuals in the difference curves probably indicate a small amount of a third morimotoite phase with a slightly smaller unit-cell parameter, which was not modeled (Figure 2).

Because the two phases are quite similar to each other, there are some correlations between the structural parameters in the two-phase refinement. Therefore, the isotropic displacement parameters for atoms in the same site were constrained to be equal to each other, and the profile parameters for both phases were also constrained to be the same. Because of the profile constraint, sample size and strain information could not be obtained for this sample. However, in other garnet samples, such information was obtained (Antao, 2013a, 2013c).

The crystal structure of morimotoite can be rationalized using bond-valence sums (BVS) calculated in valence units

(v.u.) (Wills and Brown, 1999). For the isotropic refinement using a single phase (Table V), the BVS for the Ca atom at the X site is 2.26 v.u., so the Ca atom is a bit large for the X site. For Ti^{4+} at the Y site, the BVS is 3.59 v.u. and this site also contains Fe^{3+} and Fe^{2+} cations. The BVS for Si atom at the Z site is 3.44 v.u., which is reasonable because there are some Al and Fe^{2+} cations in this site (Table I). The BVS for the O atom is 1.95 instead of 2 v.u., which is reasonable.

It is possible that formation of a two-phase intergrowth of morimotoite in Si-deficient rocks may be related to changes in oxygen fugacity (f_{O2}), activity of SiO_2 (a_{SiO2}), etc., as the crystals grow at low temperature that prevents diffusion or homogenization of the cations. The two phases cause strain that arises from structural mismatch and gives rise to optical anisotropy, as was found in other garnets (Antao, 2013a, 2013b, 2013c; Antao and Klincker, 2013a, 2013b; Antao and Round, 2014). The two-phase intergrowth in morimotoite may be similar to epitaxial intergrowths because of the similarity of the structural and chemical parameters (Kitamura and Komatsu, 1978). However, the small differences between the two phases give rise to structural mismatch that results in strain and low optical anisotropy.

ACKNOWLEDGEMENTS

The Editor J. Kaduk and three anonymous reviewers are thanked for their helpful comments on this manuscript. A. Locock is thanked for providing the Ice River sample. R. Marr is thanked for his help with the EMPA data collection. The HRPXRD data were collected at the X-ray Operations and Research beamline 11-BM, Advanced Photon Source (APS), Argonne National Laboratory (ANL). Use of the APS was supported by the US Department of Energy, Office of Science, Office of Basic Energy Sciences, under contract number DE-AC02-06CH11357. This work was supported with a NSERC Discovery Grant.

Antao, S. M. (**2013a**). "Three cubic phases intergrown in a birefringent andradite-grossular garnet and their implications," Phys. Chem. Miner. **40**, 705–716.

Antao, S. M. (**2013b**). "Can birefringent near end-member grossular be non-cubic? New evidence from synchrotron diffraction," Can. Mineral. **51**, 771–784.

Antao, S. M. (**2013c**). "The mystery of birefringent garnet: is the symmetry lower than cubic?," Powder Diffr. **28**, 265–272.

Antao, S. M. and Klincker, A. M. (**2013a**). "Origin of birefringence in andradite from Arizona, Madagascar, and Iran," Phys. Chem. Miner. **40**, 575–586.

Antao, S. M. and Klincker, A. M. (**2013b**). "Crystal structure of a birefringent andradite-grossular from Crowsnest Pass, Alberta, Canada," Powder Diffr. **29**, 20–27.

Antao, S. M. and Round, S. A. (**2014**). "Crystal chemistry of birefringent spessartine," Powder Diffr., doi: 10.1017/S0885715614000062

Antao, S. M., Hassan, I., Wang, J., Lee, P. L., and Toby, B. H. (**2008**). "State-of-the-art high-resolution powder X-ray diffraction (HRPXRD) illustrated with Rietveld structure refinement of quartz, sodalite, tremolite, and meionite," Can. Mineral. **46**, 1501–1509.

Armbruster, T. (**1995**). "Structure refinement of hydrous andradite, $Ca_3Fe_{1.54}Mn_{0.02}Al_{0.26}(SiO_4)_{1.65}(O_4H_4)_{1.35}$, from the Wessels mine, Kalahari manganese field, South Africa," Eur. J. Mineral. **7**, 1221–1225.

Armbruster, T. and Lager, G. A. (**1989**). "Oxygen disorder and the hydrogen position in garnet-hydrogarnet solid-solutions," Eur. J. Mineral. **1**, 363–369.

Armbruster, T. and Geiger, C. A. (**1993**). "Andradite crystal chemistry, dynamic X-site disorder and structural strain in silicate garnets," Eur. J. Mineral. **5**, 59–71.

Armbruster, T., Birrer, J., Libowitzky, E., and Beran, A. (**1998**). "Crystal chemistry of Ti-bearing andradites," Eur. J. Mineral. **10**, 907–921.

Ferro, O., Galli, E., Papp, G., Quartieri, S., Szakall, S., and Vezzalini, G. (**2003**). "A new occurrence of katoite and re-examination of the hydrogrossular group," Eur. J. Mineral. **15**, 419–426.

Grew, E. S., Locock, A. J., Mills, S. J., Galuskina, I. O., Galuskin, E. V., and Hålenius, U. (**2013**). "Nomenclature of the garnet supergroup," Am. Mineral. **98**, 785–811.

Henmi, C., Kusachi, I., and Henmi, K. (**1995**). "Morimotoite, $Ca_3TiFe^{2+}Si_3O_{12}$, a new titanian garnet from Fuka, Okayama Prefecture, Japan," Mineral. Mag. **59**, 115–120.

Kitamura, K. and Komatsu, H. (**1978**). "Optical anisotropy associated with growth striation of yttrium garnet, $Y_3(Al,Fe)_5O_{12}$," Kristallogr. Tech. **13**, 811–816.

Koritnig, S., Rösch, H., Schneider, A., and Seifert, F. (**1978**). "Der Titan-zirkon-granat aus den Kalksilikatfels-Einschlüssen des Gabbro im Radautal, Harz, Bundesrepublik Deutschland," Tschermaks Mineral. Petrogr. Mitt. **25**, 305–313.

Lager, G. A., Armbruster, T., and Faber, J. (**1987**). "Neutron and X-ray-diffraction study of hydrogarnet $Ca_3Al_2(O_4H_4)_3$," Am. Mineral. **72**, 756–765.

Lager, G. A., Armbruster, T., Rotella, F. J., and Rossman, G. R. (**1989**). "OH substitution in garnets: X-ray and neutron diffraction, infrared, and geometric-modeling studies," Am. Mineral. **74**, 840–851.

Larson, A. C. and Von Dreele, R. B. (**2000**). *General Structure Analysis System (GSAS)* (Los Alamos National Laboratory Report, LAUR 86–748).

Lee, P. L., Shu, D., Ramanathan, M., Preissner, C., Wang, J., Beno, M. A., Von Dreele, R. B., Ribaud, L., Kurtz, C., Antao, S. M., Jiao, X., and Toby, B. H. (**2008**). "A twelve-analyzer detector system for high-resolution powder diffraction," J. Synchrotron Radiat. **15**, 427–432.

Locock, A., Luth, R. W., Cavell, R. G., Smith, D. G. W., and Duke, M. J. M. (**1995**). "Spectroscopy of the cation distribution in the schorlomite species of garnet," Am. Mineral. **80**, 27–38.

Locock, A. J. (**2008**). "An excel spreadsheet to recast analyses of garnet into end-member components, and a synopsis of the crystal chemistry of natural silicate garnets," Comput. Geosci. **34**, 1769–1780.

Novak, G. A. and Gibbs, G. V. (**1971**). "The crystal chemistry of the silicate garnets," Am. Mineral. **56**, 1769–1780.

Peterson, R. C., Locock, A. J., and Luth, R. W. (**1995**). "Positional disorder of oxygen in garnet: the crystal-structure refinement of schorlomite," Can. Mineral. **33**, 627–631.

Rietveld, H. M. (**1969**). "A profile refinement method for nuclear and magnetic structures," J. Appl. Crystallogr. **2**, 65–71.

Shannon, R. D. (**1976**). "Revised effective ionic radii and systematic studies of interatomic distances in halides and chalcogenides," Acta Crystallogr. **A32**, 751–767.

Toby, B. H. (**2001**). "EXPGUI, a graphical user interface for GSAS," J. Appl. Crystallogr. **34**, 210–213.

Wang, J., Toby, B. H., Lee, P. L., Ribaud, L., Antao, S. M., Kurtz, C., Ramanathan, M., Von Dreele, R. B., and Beno, M. A. (**2008**). "A dedicated powder diffraction beamline at the advanced photon source: commissioning and early operational results," Rev. Sci. Instrum. **79**, 085105.

Wills, A. S. and Brown, I. D. (**1999**). VaList. CEA, France. This is a freely available computer program.